Modelling the effect of cross-field diffusion on tearing mode stability

M. James[1,2,*], H.R. Wilson[3] and J.W. Connor [2]

September 29, 2009

[1] University of Bristol, H.H. Wills Physics Laboratory, Royal Fort, Bristol, BS8 1TL

[2] EURATOM/UKAEA Fusion Association, Culham Science Centre, Abingdon, Oxon, OX14 3DB

[3] Department of Physics, University of York, Heslington, York, YO10 5DD

Abstract

The formation of neoclassical tearing modes (NTMs) severely limits the performance of a tokamak plasma by increasing the radial particle and heat fluxes from the core and can even lead to a plasma disruption. Indeed, NTMs are a serious consideration for the next step device, ITER. The appearance of a finite NTM magnetic island requires an initial "seed" island to be unstable and it is important to develop an understanding of the early evolution of this island. In this phase, the island is long and narrow and a significant contribution to its stability arises from the associated polarisation current. The effect of the polarisation current is sensitive to the plasma model used in the vicinity of the island separatrix. Here we present a gyro-kinetic calculation of the island stability that includes plasma cross-field diffusion in a narrow layer at the separatrix. The result of this is not only to smooth the density profile around the island separatrix, but also to introduce a dependence of the plasma properties on the position along the island's flux surface in that vicinity. This paper compares the island's stability with and without the diffusive layer and shows that a proper treatment of transport effects in the layer significantly reduces the impact of the polarisation current on the island's stability, at least in the parameter range considered.

1 Introduction

The closed magnetic surfaces associated with a magnetic island formed in a tokamak plasma allow rapid transport of plasma particles and energy around the island, leading to the flattening of the pressure and density profiles across it, and hence to a reduction of the bootstrap current inside the island. On the basis of a modified

*Present address: SERCO, Harwell Science and Innovation Centre, Didcot, Oxon OX11 0QB

Rutherford equation this has been shown to provide a drive for island growth [1, 2] when the magnetic shear and pressure gradient have opposite signs. More recent studies have drawn attention to the contribution of the polarisation current (which, for long narrow islands, is significant) in both slab [3, 4, 5, 6] and toroidal geometries [7, 8]. This contribution is sensitive to the modelling of the plasma behaviour near the island separatrix and can provide a stabilising or destabilising contribution for sufficiently small islands, depending on the frequency of rotation of the island relative to the plasma [9]. Most studies of the polarisation current have considered limiting cases in which the island width, w, is either large or small compared to the ion Larmor radius, ρ_i. In a recent paper [6] (see also [4, 10]) a gyro-kinetic treatment of the ions, i.e. retaining full ion Larmor radius effects, albeit in slab geometry, was presented, allowing one to study the effects of an arbitrary ratio of w/ρ_i. The impact of large ion banana orbits in a torus has also been explored [11].

The polarisation current could provide a threshold island size below which the island is stable, as has also been observed experimentally [12]. However there is another possible explanation for such a threshold. Generally, the model for the bootstrap current perturbation used in most works [1, 2, 6, 7, 8] assumes a density profile that is flattened across the whole of the island. In this case the bootstrap current deficit makes a significant contribution to the instability drive for any island size, no matter how small. However, the diffusion across flux surfaces can compete with parallel transport for sufficiently small islands, and near the separatrix of larger islands. This smooths the density and pressure somewhat and allows a pressure gradient to be supported across an island chain [13, 14]. Thus the bootstrap current is not completely "switched off" in the interior of narrow islands, which gives rise to a threshold width for instability. Gorelenkov et al [14] considered the modification to the bootstrap current contribution from this diffusion to the island stability and were able to predict the critical threshold island width, w_χ. They compared their theoretical results with data on NTMs from the TFTR experiment [15] and found that the stability criterion was violated in the cases where modes were observed. A number of studies were subsequently performed on tokamaks around the world to deduce whether the diffusion or polarisation current dominates the threshold physics. Experiments on JET [16] showed a role for both terms, while results from ASDEX Upgrade [17] and DIII-D [18] provided evidence that the threshold is proportional to the ion Larmor radius. This latter result is consistent with the ion polarisation current model, but could be a result of the diffusion model if the thermal diffusivity scales appropriately with plasma parameters. A potentially important piece of physics that has not yet been addressed by theory is how the modification to the pressure profile around the island caused by the finite cross-field diffusion influences the polarisation current. This is the purpose of the present paper.

A detailed study of cross field diffusion close to the island separatrix in both fluid [13] and kinetic models [19] has been performed previously. While the results presented in the fluid case show the expected form of the temperature perturbations (as well as providing an estimate of the peak destabilizing bootstrap contribution

to the Rutherford equation for different machine sizes), the work on the kinetic model, has not been fully exploited. The existing work has generated only the form of the distribution function in Fourier space and stopped short of determining the consequences for island stability. In this paper, therefore, we describe the methodology and consequences of incorporating the analytic work of reference [19] into the numerical model developed previously [6] to calculate the effect of diffusion on the electron distribution function and the consequences for the polarisation current. In particular we compare the use of a crude effective diffusion coefficient that smooths profiles, as employed in [6], with the results obtained here using a more rigorous treatment. The implications of this improved kinetic model for the island stability can then be assessed.

The paper proceeds in section 2 with a brief description of the magnetic topology before describing the salient features of the separatrix analysis in section 3. An overview of the previous work in the outer region, beyond the separatrix, is given in section 4 before the scheme used to match the layer to the outer region is presented in section 5. The results for the density distribution are outlined in section 6 and the implications for the polarisation current and its impact on island stability are given in section 7. We do not address the self-consistent determination of the island rotation frequency from torque balance, treating this as a given parameter when studying the island stability through the Rutherford equation for the island width. There is a discussion of the limitations on the calculation in section 8 while their implications, together with a summary, are addressed in section 9.

2 Magnetic topology

The work presented in this paper uses a sheared slab model of the plasma and, as such, has a magnetic field given by

$$\boldsymbol{B} = B_0 \left[\nabla z - \nabla\psi \times \nabla z\right], \tag{1}$$

with B_0 the equilibrium field. A coordinate system consisting of the orthogonal directions $\nabla z, \nabla\xi$ and ∇x is used. The island is modelled by the inclusion of a helical perturbation with the form $A_\parallel = -\tilde{\psi}\cos m\xi$, where $A_\parallel$ is the parallel vector potential and the resulting total flux is given by

$$\psi = -\frac{x^2}{2L_s} + \tilde{\psi}\cos m\xi. \tag{2}$$

Here $\tilde{\psi} = w^2/4L_s$ is the perturbed flux and $w = \sqrt{4L_s\tilde{\psi}}$ is the island half width. This island model could be considered to mimic an island in a torus if we regard ξ as the angular variable

$$m\xi = m\left(\theta - \frac{\varphi}{q(r_0)}\right) - \int^t \omega\left(t'\right) dt', \tag{3}$$

where θ and φ are the poloidal and toroidal angles of the torus that has been deformed to produce the slab geometry and m is the poloidal mode number of the island structure, while $q(r_0)$ is the safety factor at the resomant surface r_0 (where $lq(r_0) = m$ for some integer l) and ω is the island rotation frequency. It is also convenient to define a dimensionless flux-surface label,

$$\Omega = -\frac{\psi}{\tilde{\psi}} \equiv \frac{2x^2}{w^2} - \cos m\xi. \tag{4}$$

This definition is such that $\Omega = -1$ is the O-point, $\Omega = 1$ corresponds to the separatrix and $\Omega > 1$ denotes the region outside the island.

3 The separatrix layer

We shall use a kinetic model for the electrons in the vicinity of the separatrix. Following the work of reference [19], the cross-field diffusion coefficient, D (caused by small scale plasma turbulence, for example), is introduced as a leading order term in the electron kinetic equation and allowed to compete on an equal footing with the parallel streaming term, while collisions and drifts due to finite Larmor radius effects are neglected. (We are therefore assuming the transit time around the island is much greater than the characteristic time step in the random walk of the particles underlying the diffusive process.) Normally the diffusive terms would be negligible but close to the separatrix the scale length for variations across the magnetic field, L_r, is also very small, enhancing the effect of cross-field diffusion. The length scale L_r (i.e. the width of the separatrix layer) is given by the balance

$$\frac{D}{L_r^2} \sim \frac{v_{th,e}}{L_\parallel}, \tag{5}$$

where $v_{th,e}$ is the electron thermal velocity and D is the diffusion coefficient. The parallel scale length is given by $L_\parallel$ and is the characteristic length of a magnetic field line for one turn around the island, i.e. $L_\parallel \sim 2\pi L_s/k_\theta w$, where $L_s = Rq/s$ with R the major radius of the tokamak (a is the plasma minor radius and r the radius of a given flux surface), $k_\theta = m/r$ and $s = (r/q)(dq/dr)$ is the magnetic shear. This parallel scale length is assumed to be much greater than the island half-width, w, so that we can introduce the ordering

$$L_\parallel \gg w \gg L_r. \tag{6}$$

Thus the drift kinetic equation for electrons can be expressed as

$$v_\parallel \nabla_\parallel f_j = \boldsymbol{\nabla} \cdot (D \boldsymbol{\nabla} f_j)\,, \tag{7}$$

where the subscript $\parallel$ is used to denote the component of a vector parallel to the magnetic field direction and j is the species label. It can be shown that the distribution function, f_j, is equivalent to the function $h\,(\Omega)$ used in previous work [6, 7].

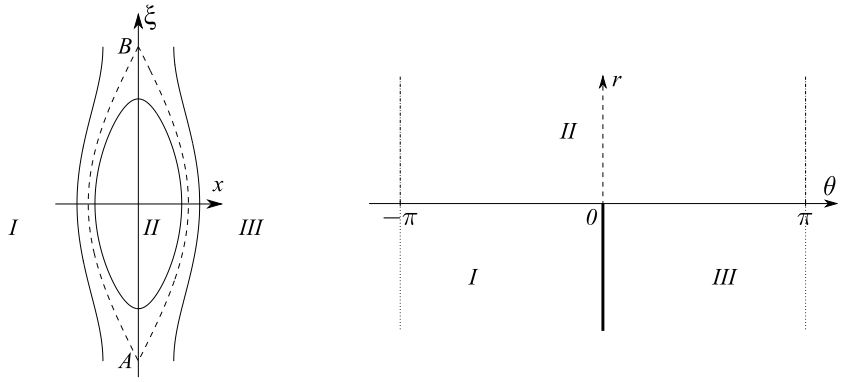

(a) The island with the X-points marked A and B.

(b) The island in the transformed space with the new coordinates r and θ marked.

Figure 1: A pictorial representation of the transformation from (x, ξ) coordinates to (r, θ) coordinates.

The parallel electric field term, $(e/mv)v_{\|}E_{\|}\left(\partial f/\partial v\right)$, has been neglected to simplify the analysis. While this may not be entirely valid in the diffusive layer, the key purpose of this work is to provide the first step towards a complete solution, identifying the essential impact of diffusion on the density, plasma flow and polarisation current. Thus the results presented here will be important in determining if the diffusion has a significant effect on the island stability. The inclusion of the parallel electric field is left to future work; however, the likely importance of this approximation is assessed a posteriori in section 8.

Figure 1 illustrates the coordinate transformation from the conventional (x, ξ) coordinates of the slab geometry to the (r, θ) system of reference [19]. This transformation is equivalent to opening out the island so that the O-point is given by $(r = \infty, \theta = 0)$ while the line $r = 0$ marks the separatrix. For the model to be valid, the bold line $\theta = 0, r < 0$ must be impenetrable to particles as it is the boundary between the plasma on either side of the island and it is impossible for particles to move between these two regions without passing through region II.

In this transformation r is given by

$$r = \frac{\sqrt{\pi m}}{2}\left(\frac{w^3 u}{L_s a D}\right)^{1/2}\int_{\kappa}^{1}\frac{\kappa^{1/2}}{[E(\kappa^{-2})]^{1/2}}d\kappa \tag{8}$$

outside the island and by

$$r = \frac{\sqrt{\pi m}}{2}\left(\frac{w^3 u}{L_s a D}\right)^{1/2}\int_{\kappa}^{1}\frac{\kappa d\kappa}{\sqrt{E\left(\kappa^2\right)+\left(\kappa^2-1\right)K\left(\kappa^2\right)}} \tag{9}$$

inside, where $v_{\|} = \sigma u$ with $\sigma = \pm 1$ and $K\left(\kappa^2\right)$ and $E\left(\kappa^2\right)$ are the complete elliptic integrals of the first kind and second kinds, respectively. Here $\kappa^2 =$

$(-4L_s\psi + w^2)/2w^2$, while the angular variable, θ, is defined by

$$\theta = \frac{\pi}{2}\frac{E\left(\beta, \kappa^{-2}\right)}{E\left(\kappa^{-2}\right)} + c_I \tag{10}$$

outside the island, where $\beta = m\xi/2$. Inside the island, the form of θ is altered to account for the fact that ξ no longer varies over the full range:

$$\theta = \frac{\pi}{2}\frac{\left(\kappa^2 - 1\right)K\left(\varphi, \kappa^2\right) + E\left(\varphi, \kappa^2\right)}{\left(\kappa^2 - 1\right)K\left(\kappa^2\right) + E\left(\kappa^2\right)} + c_I, \tag{11}$$

where $K\left(\varphi, \kappa^2\right)$ and $E\left(\varphi, \kappa^2\right)$ are elliptic integrals and c_I is a constant of integration that can be determined from the coordinate transformation. For the island illustrated in Figure 1(a), with the X-points at $m\xi = \pm\pi$, it is clear that $c_I = \pi/2$.

Writing

$$\frac{\partial f}{\partial \psi} = \frac{\partial r}{\partial \psi}\frac{\partial f}{\partial r} + \frac{\partial \theta}{\partial \psi}\frac{\partial f}{\partial \theta}, \tag{12}$$

and noting that the second term on the right hand side is small enough to be neglected in all but a very narrow neighbourhood of the separatrix (see below), it is found that the kinetic equation, Eq.(7), becomes

$$\frac{\partial f}{\partial \theta} = \sigma\frac{\partial^2 f}{\partial r^2}. \tag{13}$$

An important assumption in the consistency of our ordering scheme is that the island half-width, w, is much greater than the separatrix layer, $w \gg L_r$, which in turn requires that

$$w \gg \left(\frac{DaL_s}{v_{th,e}}\right)^{1/3}. \tag{14}$$

With this ordering satisfied, it can be assumed that $x \sim w$ and $\kappa \sim 1$ throughout the region of interest, including the region where $r \gg 1$.

For the above orderings to be meaningful, the neglect of the second term in Eq.(12) must be justified, which requires

$$\frac{\partial \ln f}{\partial \psi} \gg \frac{\partial \theta}{\partial \psi}, \tag{15}$$

where it has been assumed that $\partial f/\partial\theta \sim f$. This ordering has been shown to be satisfied in all but an exponentially narrow region around the separatrix [19]. Since this layer is much narrower than the diffusive layer the equations presented are sufficiently accurate for the calculations considered here.

3.1 Fourier space analysis

To solve the differential equation Eq.(13) we closely follow the approach of reference [19], transforming it into Fourier space to give

$$\frac{\partial F}{\partial \theta} = -\sigma k^2 F, \tag{16}$$

which has the solution

$$F(k,\theta,\sigma) = F_{0^-}(k,\sigma)\, e^{-\sigma k^2 \theta}, \qquad \theta < 0, \tag{17}$$

$$F(k,\theta,\sigma) = F_{0^+}(k,\sigma)\, e^{-\sigma k^2 \theta}, \qquad \theta > 0, \tag{18}$$

where F_{0^+} is used for $\theta > 0$ while F_{0^-} is appropriate for $\theta < 0$.

The full analytic forms of the Fourier transformed distribution function for both $\theta < 0$ and $\theta > 0$ are determined by the Wiener-Hopf technique as:

$$F_{0^-} = \frac{\sigma C_\sigma}{V_l(k)} \left[1 + \sigma V(k)\right] e^{-\sigma \pi k^2} \tag{19}$$

$$F_{0^+} = \frac{\sigma C_\sigma}{V_l(k)} \left[\sigma V(k) - 1\right] e^{\sigma \pi k^2} \tag{20}$$

where

$$V(k) \equiv \frac{V_l(k)}{V_u(k)} = \tanh\left(\pi k^2/2\right) \tag{21}$$

and V_l (V_u) is analytic in the lower (upper) half plane. Substituting this into Eq.(17) and Eq.(18) respectively, yields

$$F(k,\theta,\sigma) = \frac{\sigma C_\sigma e^{-\sigma k^2(\theta+\pi/2)}}{V_l(k)\cosh(\pi k^2/2)}, \qquad \theta < 0 \tag{22}$$

$$F(k,\theta,\sigma) = -\frac{\sigma C_\sigma e^{-\sigma k^2(\theta-\pi/2)}}{V_l(k)\cosh(\pi k^2/2)}, \qquad \theta > 0. \tag{23}$$

where the definition of V_l has been taken from reference [19]:

$$V_l(k) = \frac{k^2}{k-i} e^{-q_l(k)}. \tag{24}$$

Substituting for V_l and introducing $q_l(0)$, where

$$q_l(0) = -\frac{1}{2}\ln\frac{\pi}{2}. \tag{25}$$

gives

$$F(k,\theta,\sigma) = \frac{k-i}{k^2}\sigma C_\sigma \frac{2e^{-\sigma k^2(\theta+\pi)}}{1+e^{-\sigma\pi k^2}} e^{q_l(k)}, \qquad \theta < 0 \tag{26}$$

$$F(k,\theta,\sigma) = -\frac{k-i}{k^2}\sigma C_\sigma \frac{2e^{-\sigma k^2\theta}}{1+e^{-\sigma\pi k^2}} e^{q_l(k)}, \qquad \theta > 0, \tag{27}$$

3.2 Transformation back to real space

Having established an analytic form for the distribution function in Fourier space, the inversion of the Fourier transform must now be performed. The form of F,

however, means that this must be done numerically. It is noted that the inverse transform of Eq.(16) yields

$$\frac{\partial f}{\partial \theta} = -\frac{\sigma}{2\pi}\int_{-\infty}^{\infty} dk e^{-ikr} k^2 F\left(k,\theta,\sigma\right) \tag{28}$$

where k^2F is regular for all real k, unlike F itself. However an analytic expression can be obtained far from the separatrix outside the island, where it takes the form given by reference [19]:

$$\lim_{x\to\infty} f_{layer} = -c_1 F_0 \left(\left(uw^3\pi/L_s a D\right)^{1/2} \frac{1}{8}\left(\Omega - 1\right) - \alpha \right). \tag{29}$$

where F_0 is a Maxwellian given by

$$F_0 = \frac{1}{\pi^{3/2} v_{th,e}^3} e^{-\left(v/v_{th,e}\right)^2}, \tag{30}$$

Clearly this distribution function does not have a Maxwellian form because of the dependence on the velocity u in the brackets, as shown in Figure 2.

4 The outer layer

Further from the island, cross-field diffusion no longer dominates collisions, which tend to drive the solution to a Maxwellian form. The electron distribution f then satisfies the equation

$$k_\| v_\| \left.\frac{\partial f}{\partial \xi}\right|_\Omega = -D\frac{\partial^2 f}{\partial r^2} + \nu\left(f - nF_0\right) \tag{31}$$

where $k_\| = -mx/rL_s$, a number conserving Krook collision operator with a collision frequency ν is used and n is the density. In order to evaluate the density profile, Eq.(31) is solved far from the island where the diffusion can be treated perturbatively [7]. The leading order solution is then $f = n\left(\Omega\right)F_0$ with the density, n, undetermined. The diffusion is subsequently introduced at first order and, by annihilating the parallel streaming term acting on the first-order distribution, the form of n is found from the solubility condition for the first-order solution, as shown later in this section. This solution for n has a discontinuity in the density gradient at the island's separatrix. This is resolved through the introduction of the cross-field diffusion in the layer near the separatrix as discussed in section 3. However, as we have seen, the solution in this layer is not Maxwellian and therefore cannot be matched directly to our outer solution.

To resolve this, an intermediate matching region is introduced where the free streaming dominates while the collisions and diffusion appear at a comparable level in next order (i.e. the successive terms in Eq.(31) are ordered as $1 : \varepsilon : \varepsilon$, where we

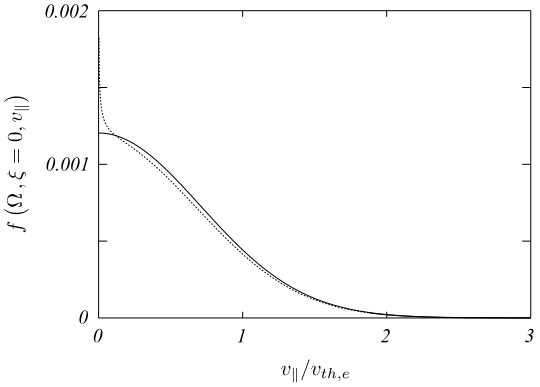

Figure 2: The electron distribution function across the island O-point near the separatrix (dashed line) and far from it (full line). The full line is a Maxwellian while the dashed line is clearly not.

indicate orders by the small parameter ϵ). The function f may then be expanded in terms of this small parameter and terms of equal order matched:

$$f = f^{(0)} + \varepsilon f^{(1)} + \cdots \tag{32}$$

$$O(1) \qquad k_\parallel v_\parallel \left.\frac{\partial f^{(0)}}{\partial \xi}\right|_\Omega = 0 \tag{33}$$

$$\Rightarrow f^{(0)} = f^{(0)}(\Omega) \tag{34}$$

$$O(\varepsilon) \qquad k_\parallel v_\parallel \left.\frac{\partial f^{(1)}}{\partial \xi}\right|_\Omega = -D\frac{\partial^2 f^{(0)}}{\partial r^2} + \nu\left(f^{(0)} - nF_0\right) \tag{35}$$

Averaging over ξ at fixed Ω and assuming $f^{(1)}$ to be periodic in ξ, yields

$$-D\left\langle \frac{\partial^2 f^{(0)}}{\partial r^2} \right\rangle_\Omega + \nu\left(f^{(0)} - nF_0\right) = 0 \tag{36}$$

where

$$\langle \cdots \rangle_\Omega = \frac{\oint \cdots [\Omega + \cos\xi]^{-1/2}\, d\xi}{\oint [\Omega + \cos\xi]^{-1/2}\, d\xi}. \tag{37}$$

Given $\Omega = 2(x/w)^2 - \cos\xi$, $\partial^2 f/\partial r^2$ can be written as

$$\frac{\partial^2 f}{\partial r^2} = \frac{\partial \Omega}{\partial r}\frac{\partial}{\partial \Omega}\left[\frac{\partial \Omega}{\partial r}\frac{\partial f}{\partial \Omega}\right] = \frac{8}{w^2}\sqrt{\Omega + \cos\xi}\frac{\partial}{\partial \Omega}\left[\sqrt{\Omega + \cos\xi}\frac{\partial f}{\partial \Omega}\right], \tag{38}$$

and substituting this into Eq.(36), it is found that

$$\frac{8}{w^2} D \frac{d}{d\Omega}\left(Q\frac{df^{(0)}}{d\Omega}\right) = P\nu\left(f^{(0)} - nF_0\right), \tag{39}$$

where

$$P = \frac{1}{2\pi}\int_{-\pi}^{\pi}\frac{d\xi}{\sqrt{\Omega+\cos\xi}} \qquad ,Q = \frac{1}{2\pi}\oint\sqrt{\Omega+\cos\xi}d\xi. \tag{40}$$

We introduce the quantities, $\hat{\nu}$ and z, where

$$\hat{\nu} = \frac{\nu w^2}{8D}, \qquad z = \int_1^{\Omega}\frac{d\Omega}{Q} \tag{41}$$

and z has been defined in such a way that $z = 0$ at the separatrix flux surface $\Omega = 1$. This allows Eq.(39) to be rewritten involving the small collisionality parameter $\hat{\nu}$:

$$\frac{d^2 f}{dz^2} = \hat{\nu}PQ\left(f - nF_0\right). \tag{42}$$

Noting that $\int d^3v f = n$, and $\int d^3v F_0 = 1$, we find

$$\frac{d^2 n}{dz^2} = 0 \qquad \Rightarrow n = az + b \tag{43}$$

and the boundary condition at large z allows the coefficient a to be determined. In the limit that x tends to infinity, the density varies on the equilibrium scale length, satisfying $d(lnn_0)/dr = 1/L_n$, with n_0 the equilibrium density near the island, and thus from Eq.(43) it follows that

$$n = \frac{1}{2\sqrt{2}}\frac{w}{L_n}\int_1^{\Omega}\frac{d\Omega}{Q} + b = h(\Omega) + b, \tag{44}$$

where b is a constant of integration. The equations are unchanged by the addition of a spatially constant Maxwellian to the distribution, f, and it is conventional to treat the density at the O-point ($\Omega = -1$) as 0 so that b is just the density at the separatrix ($\Omega = 1$). The integral term is identical to the function $h\left(\Omega\right)$ discussed in reference [7], and models the density profile in the vicinity of the island (outside the saparatrix layer). In reference [7] the density was taken to be flat across the island region and consequently the constant of integration, b, was zero. In this new formalism, however, diffusion across the island region is included with the result that the distribution function must join smoothly onto the island region. This matching determines b, which is not zero in general. In the following section we determine b and the other parameters required to match the two forms of f.

With Eq.(43) in mind we first introduce a new distribution function, $\tilde{f} = f - nF_0$, so that Eq.(42) can be rewritten as

$$\frac{d^2\tilde{f}}{dz^2} = \hat{q}^2\tilde{f}, \qquad \hat{q}^2 = \hat{\nu}PQ. \tag{45}$$

5 Matching the two solutions

We first consider the conditions that allow the two solutions to be matched in a common region of validity. Earlier work [6] used a standard drift wave ordering scheme with

$$k_\parallel v_{th,e} \gg \omega \gg k_\parallel v_{th,i} \tag{46}$$

where $\omega \sim \omega_{*,j} = -k_\theta T_j/e_j B L_n$ is the island frequency and j denotes the species. Substituting these definitions into Eq.(46), taking $x \sim w$ and noting $v_{th,j}\rho_j = 2T_j/e_j B$ yields

$$2\frac{L_s}{L_n}\rho_e \ll w \ll 2\frac{L_s}{L_n}\rho_i \tag{47}$$

setting an upper and a lower limit on the island size. Comparing this with the minimum island width of reference [19],

$$w \gg \left(\frac{aL_sD}{v_{th,e}}\right)^{1/3} \tag{48}$$

it is found that

$$\left(\frac{aL_sD}{v_{th,e}}\right)^{1/3} \ll w \ll 2\frac{L_s}{L_n}\rho_i \tag{49}$$

which requires

$$D \ll 5\times 10^2(\rho_i/a)D_{gB}. \tag{50}$$

Here $D_{gB} \sim v_{th,i}\rho_i^2/L_n$ is the gyro-Bohm diffusion coefficient, and the following assumptions have been made: $L_s/L_n \equiv Rq/sL_n \sim 10$ where $R/L_n \sim 3$ is the ratio of major radius to density scale length, $q \sim 3$ is the safety factor and $s \sim 1$ is the magnetic shear parameter. Equation (50) is generally satisfied for tokamak plasmas.

5.1 The outer solution

Equation (45) is completely general and, assuming $\hat{\nu} \gg 1$, a solution can be found using WKB theory

$$\tilde{f} \approx (f_0 + f_1 + \cdots)\, A e^{-\int_0^z dz'\hat{q}} \tag{51}$$

$$\Rightarrow \frac{d\tilde{f}}{dz} = \left\{-\hat{q}\,(f_0 + f_1 + \cdots) + f_0' + f_1' + \cdots\right\} e^{-\int_0^z dz'\hat{q}} \tag{52}$$

$$\Rightarrow \frac{d^2\tilde{f}}{dz^2} = A\left\{\hat{q}^2\,(f_0 + f_1 + \cdots) - 2\hat{q}\left(f_0' + f_1' + \cdots\right) + f_0'' + f_1''\right\} A e^{-\int_0^z dz'\hat{q}}$$
$$+ \left\{\cdots - \hat{q}'\left(f_0' + f_1' + \cdots\right)\right\} A e^{-\int_0^z dz'\hat{q}}. \tag{53}$$

Substituting Eqs.(51) and (53) back into Eq.(45), it is found that to leading order

$$2\hat{q}\frac{df_0}{dz} + \frac{d\hat{q}}{dz}f_0 = 0 \qquad \Rightarrow f_0 = \hat{q}^{-1/2}. \tag{54}$$

which is the usual WKB structure. Thus the form for f and its derivative is determined and this can be matched to the solution in the separatrix region:

$$\begin{aligned} f &= \left[\frac{1}{2\sqrt{2}}\frac{w}{L_n}\int_1^{\Omega}\frac{d\Omega}{Q}+b\right]F_0 \\ &+ \left(\hat{q}^{-1/2}+f_1+\cdots\right)Ae^{-\int_0^z \hat{q}dz'}, \end{aligned} \tag{55}$$

$$f\left(z=0\right) = bF_0 + A\left[\hat{q}_0^{-1/2}+f_1\left(0\right)\right], \tag{56}$$

$$\left.\frac{df}{dz}\right|_{z=0} = \frac{F_0}{2\sqrt{2}}\frac{w}{L_n} + A\left\{-\hat{q}_0\left[\hat{q}_0^{-1/2}+f_1\right]+\left[-\frac{1}{2}\hat{q}_0^{-3/2}\hat{q}_0'+f_1\right]\right\}, \tag{57}$$

where $\hat{q}_0$ is $\hat{q}$ evaluated at the separatrix. It is noted here that the condition $\hat{\nu} \gg 1$ means that the contribution from the exponential term will die off very quickly and it is expected to be important in only a very small region: the matching region.

5.1.1 The numerical method

It is known that the solution for the outer region has the form

$$f = \left[h(\Omega)+b\right]F_0 + A(v)g\left(\Omega\right), \tag{58}$$

where A is a function of v only and the Ω dependence of the last term is contained entirely within g (which is known from the WKB analysis above to be an exponentially decaying function). This exponentially decaying piece is precisely the function $\tilde{f}$ discussed earlier and, as such, must satisfy Eq.(45), expressed in terms of Ω by

$$\frac{d}{d\Omega}\left(Q\frac{d\tilde{f}}{d\Omega}\right) = P\hat{\nu}\tilde{f}. \tag{59}$$

In order to determine $\tilde{f}$ numerically, two independent solutions of this second order equation are introduced, defined by their behaviour at the origin:

$$g_1(1) = 0 \quad g_1'(1) = 1, \tag{60}$$

$$g_2(1) = 1 \quad g_2'(1) = 0, \tag{61}$$

where the prime denotes a derivative with respect to Ω and we recall that $\Omega = 1$ labels the separatrix. These solutions will then be combined appropriately to exclude the exponentially growing solution of $\tilde{f}$:

$$\tilde{f} = A\left(v\right)g; \quad g = a_1g_1 + a_2g_2 \tag{62}$$

Using this numerical scheme, the functions g_1 and g_2 can be obtained. Applying the boundary conditions that the function g (see Eq.(62)) must tend to zero at infinity and that it is 1 at the separatrix, determines the correct combination ofg_1 and g_2 and the parameter a_1 is then obtained (clearly $a_2 = 1$). Specifically, the ratio of g_1 and g_2 at "infinity" (namely the edge of the box used in the numerical analysis) then determines a_1.

5.2 Matching close to the separatrix

It is known that the distribution function in the separatrix region is a function not only of the flux surface, but also of the distance along the island (the angular variable, ξ). This makes matching exactly at the separatrix impossible, and instead the matching is performed at an intermediate point where the two solutions have a common region of validity. The scale length for variations perpendicular to the magnetic field is given by [19],

$$\frac{L_r}{w} = \sqrt{\frac{DaL_s}{w^3 v_{th,e}}} \tag{63}$$

and we apply the matching some number of these scale lengths away from the separatrix, where the angular (i.e. ξ) variations in f_{layer} have died away.

The solution for the outer region is known to have the form given in Eq.(58), where the exponentially decaying piece, g, has been determined using the numerical method described in section 5.1.1. Solution (58) is then matched to the asymptotic form for the separatrix region at large r,

$$\lim_{x\to 1} f_{sep} = -c_1(r-\alpha)F_0 \equiv -c_1 C u^{1/2} F_0 \left(1 - \sqrt{\frac{\Omega+1}{2}}\right) + \alpha c_1 F_0, \tag{64}$$

where $C = 0.5\left(w^3\pi/L_s a D\right)^{1/2}$. (This reduces to the form in Eq.(29) when $\Omega \sim 1$.) As before, the values and gradients of the outer region and the separatrix region are matched, this time at the point $\Omega = 1+\delta$, where $\delta \ll 1$ is several normalised scale lengths, giving

$$c_1\left\{\alpha - Cu^{1/2}\left(1-\sqrt{1+\frac{\delta}{2}}\right)\right\} = \left(h\left(\Omega\right)+b\right) + A\left(v\right)g\left(\Omega\right), \tag{65}$$

$$\frac{dh\left(\Omega\right)}{d\Omega}F_0 + A\left(v\right)\frac{dg\left(\Omega\right)}{d\Omega} = \frac{1}{4}Cu^{1/2}\left(1+\frac{\delta}{2}\right)^{-1/2} c_1. \tag{66}$$

Manipulating these equations, we obtain the following forms for A, b and c_1,

$$A = \frac{S_1\left(h\left(\Omega\right)+b\right) - S_2 h'\left(\Omega\right)}{S_2 g'\left(\Omega\right) - S_1 g\left(\Omega\right)}F_0, \tag{67}$$

$$b = \frac{I_0}{I_1}, \tag{68}$$

$$c_1 = \frac{\left(h\left(\Omega\right)+b\right)F_0 + A\left(v\right)g\left(\Omega\right)}{S_2}, \tag{69}$$

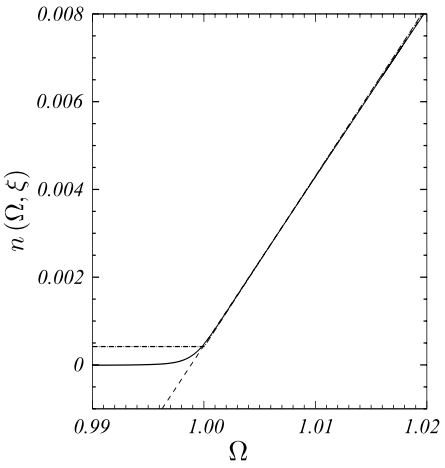

(a) The density relative to that at the island 0-point: the numerically determined "inner" solution (full line) and the "outer" solution given by the function $h(\Omega)$ shifted by the amount b (- - -), Eq.(44). The asymptotic form of the inner density is found from Eq.(74) $(--)$

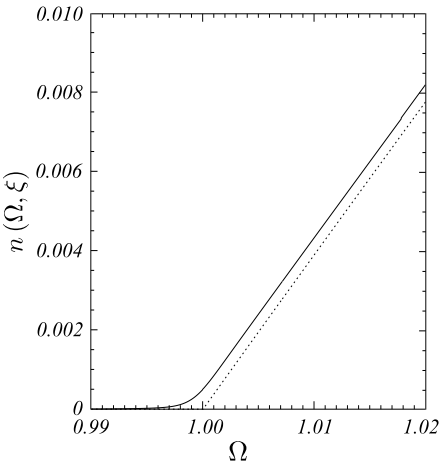

(b) The density relative to that at the island 0-point, with (full line) and without $(--)$ the diffusive layer.

Figure 3: Showing the matching of the outer and separatrix solutions and the effect this has on the density profile. Both plots are across the island O-point.

where the primes are again used to denote derivatives with respect to Ω and

$$S_1 = \frac{1}{4}Cu^{1/2}\left(1+\frac{\delta}{2}\right)^{-1/2}, \tag{70}$$

$$S_2 = \alpha - Cu^{1/2}\left(1-\sqrt{1+\frac{\delta}{2}}\right), \tag{71}$$

$$I_0 = \int \frac{S_2 h'(\Omega) - S_1 h(\Omega)}{S_2 g'(\Omega) - S_1 g(\Omega)} F_0 d^3v, \tag{72}$$

$$I_1 = \int \frac{S_1 F_0}{S_2 g'(\Omega) - S_1 g(\Omega)} d^3v. \tag{73}$$

6 Determination of the density

Having calculated the distribution function for the separatrix region and matched it to that for the outer region, the density can be obtained by integration over all velocities. Rather than match for each velocity, it is computationally simpler to first carry out the velocity integration and then match the densities. Figure 3(a) shows the resulting matching of the densities using the scheme described above. Here the full line shows the numerically determined form of the density in the separatrix region while the dot-dash line is the function $h(\Omega)$ shifted by the amount b and the

dashed line is the asymptotic form,

$$\begin{aligned}\lim_{x\to\infty} n_{sep} &= \int d^3v f_{sep} \\ &\equiv -C\left(1-\sqrt{\frac{\Omega+1}{2}}\right)\int d^3v c_1 F_0\sqrt{v_\parallel}+\alpha\int d^3v F_0 c_1, \quad (74)\end{aligned}$$

where we have used the form of f_{sep} given in Eq.(64).

A plot indicating how the diffusion affects the density around the island is shown in Figure 3(b). The dashed line shows the density without any diffusive effects incorporated while the full line shows the effect of including them. The result of their inclusion is that the density profile matches smoothly onto the island interior whereas previously it took a zero value for all $\Omega < 1$ and this led to a discontinuity in the radial derivative at the island's separatrix.

It is noted here that, although the function $A(v)$ is important for the matching of the distribution function, it makes no contribution to the density. This has been checked computationally and found to be the case, as required.

6.1 Consequences of the diffusion

The inclusion of the diffusive layer has three important consequences

- the distribution function is not Maxwellian in the diffusive layer;
- the density profile matches smoothly onto the island region; and
- the density is no longer a flux surface function in the vicinity of the island separatrix.

While the non-Maxwellian form of the distribution function has been dealt with in section 4 and motivates the introduction of the matching region described in section 5, little has been said of the profile smoothing or the deviation of the profiles from being flux-surface functions.

In the earlier model of reference [6], the density was assumed to be zero at all points within the island. In contrast, the colour contour plot of the density, illustrated in figure 4, clearly shows that the inclusion of the cross-field diffusion leads to the smoothing of the profiles into the island region. This has the effect of removing the unphysical spike from the radial derivative of the density that was present in reference [6] (the X-points are the sole exceptions and this is discussed further in section 8). In Figure 4 the line $\Omega = -\cos m\xi$ is marked and represents the edge of the physical region: inside the island, the flux surfaces do not extend all the way to $\xi = \pm m\pi$, but only to $m\xi = \pm\arccos\Omega$. The third consequence of considering the diffusive layer, namely the deviation of the density from a flux-surface quantity, can also be seen in Figure 4.

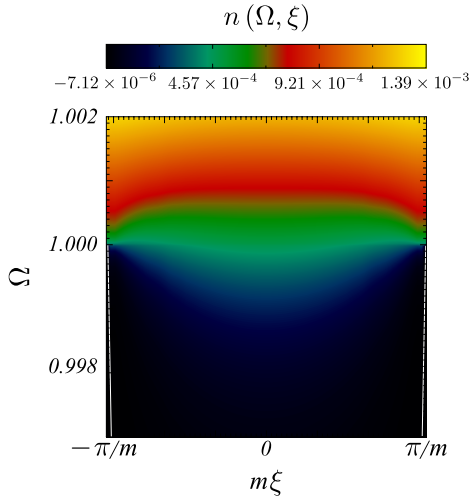

Figure 4: The density contours (relative to the value at the island 0-point) close to the island separatrix (i.e. in the diffusive layer). It can clearly be seen that the density is no longer a flux surface quantity. The white lines indicate the boundary of the physically valid region.

7 Polarisation current and island stability

This new result for the density distribution allows the re-calculation of the polarisation current and hence its effect on the island stability parameter, Δ_{pol}, to be re-evaluated. This requires the determination of the electrostatic potential which is calculated from the quasi-neutrality condition as in earlier work [6]. However, the form of the polarisation current determined in reference [6] is not accurate in the separatrix layer. The derivation of the current in this layer has to be reconsidered (see Appendix) and this results in

$$\frac{1}{n_0 e c_s} J_{\parallel}^{pol} = 4 \frac{L_s}{L_n} \frac{\rho_s}{w} \left(\hat{\omega}\tau + 1\right) \left[I_J - \langle I_J \rangle_\Omega\right] \tag{75}$$

where

$$I_J = \int_0^\xi d\xi' \left[\frac{\partial \bar{\phi}}{\partial \Omega} \frac{\partial h}{\partial \xi'} - \frac{\partial h}{\partial \Omega} \frac{\partial \bar{\phi}}{\partial \xi'}\right]. \tag{76}$$

Here we have defined $\hat{\omega} = \omega/\omega_{*,e}$ and $\tau = T_e/T_i$, while c_s is the ion sound speed and ρ_s the ion Larmor radius evaluated at this speed. Having determined the current, it can then be inserted into the expression

$$\Delta_{pol} = \frac{4}{c\tilde{\psi}} \int_{-\pi/m}^{\pi/m} \int_{-\infty}^{\infty} J_{\parallel}^{pol} \cos m\xi dx d\xi. \tag{77}$$

The parameter Δ_{pol} then yields the contribution of the polarisation current to the island's stability:

$$\frac{dw}{dt} = \Delta' + \Delta_{pol}. \tag{78}$$

where Δ' is the standard Rutherford stability parameter measuring the drive for a tearing mode arising from the equilibrium current density [20]. Scans of Δ_{pol} over the parameter space similar to those shown in reference [6] using a smoothing function, could be presented again here but this is not expected to be particularly instructive. It can be seen from Eq.(75) that the current will still be zero when $\hat{\omega}\tau = -1$ and the results of adding the smoothing function suggest that it is not the character, but the magnitude of the contribution that will be affected by the inclusion of the cross-field diffusion. Instead, it is of interest to plot the calculated form of Δ_{pol} with the diffusive term included and compare it to the form obtained with the smoothing function. This will enable us to assess the impact of the diffusion process on Δ_{pol} and the validity of using the smoothing function to mimic the effects of the diffusive layer.

The magnitude of the diffusion coefficient D is estimated using the approach of reference [13], but for ITER-like parameters. Thus the electron temperature is taken to be $T_e \sim 30$keV and the density is assumed to be $n_e \sim 1 \times 10^{20} m^{-3}$. However, since Eq.(7) balances the cross-field diffusion with the parallel streaming rather than with the parallel collisional diffusion as in reference [13], the calculation must be modified. Considering Eq.(7) we have

$$k_{\|} v_{th,e} \sim \frac{D}{x^2} \tag{79}$$

and this leads to an estimate for the smoothing parameter α introduced in reference [6]:

$$\alpha \sim \frac{mq}{16} \epsilon s \frac{r v_{th,e}}{D} \left(\frac{w}{r}\right)^3, \tag{80}$$

where $k_{\|} \sim k_\theta w / L_s$, $k_\theta = m/r$ and $L_s = Rq/s$ have again been used. The result is an equation linking D and the smoothing parameter α :

$$D_\perp \sim \alpha^{-1} \mathrm{m}^2 \mathrm{s}^{-1}, \tag{81}$$

Here the island width has been taken to be $\sim$ 2cm at a minor radius of $r \sim 1$m and, since the major radius of ITER is 6.2m, $\epsilon s \sim 1/6$. From Eq.(81) it can be seen that for realistic values of D the parameter α will be $\sim O(1)$.

Figure 5 shows the values of Δ_{pol} determined using the smoothing function compared to the values obtained with the diffusive layer included, for the case $\hat{\rho}_i = 0.1$, where $\hat{\rho}_i = \rho_i / w$. The results shown previously in Figures 3 and 4 indicate that the cross-field diffusion has not only smoothed the density profile, but also changed its form so that it is no longer a flux surface function, an effect not present in the smoothing model. Also, the separatrix layer in the present model supports a component of electric field parallel to the magnetic field (this is not the case with the smoothing model). Finally, it has been shown (Figure 2) that the distribution is no longer a Maxwellian in the separatrix layer, only matching to one successfully further from the island. The result of these changes is a reduction of the contribution of the separatrix layer to the polarisation current. Indeed, the contribution from the layer and the contribution from outside the layer almost balance

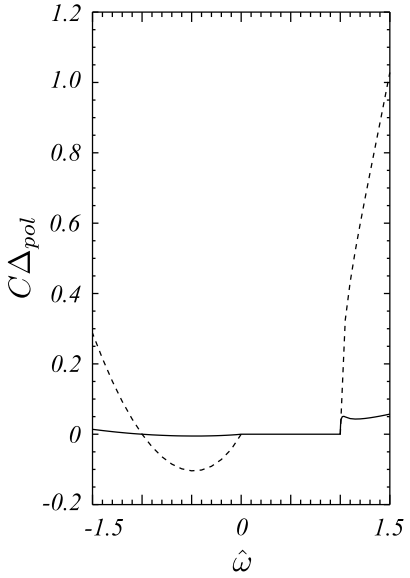

Figure 5: The effects of including cross-field diffusion (full line) in comparison with the use of the smoothing parameter α (dashed line). The dashed line shows the variation of Δ_{pol} with $\hat{\omega}$ for $\alpha = 10$, $\hat{\rho}_i = 0.1$, $\tau = 1$ and $\eta_i = L_n/L_{T_i} = 0$ for the smoothing model case, while the full line shows the effect of including the cross-field diffusion. In this case, D is chosen to be 0.1, $w^2/aL_s = 7.2 \times 10^{-4}$ and $\hat{\nu} = 3.33$.

now because they have opposite signs, so the magnitude of Δ_{pol} is reduced over the full range of $\hat{\omega}$. This is a sigificant result since it suggests that seed islands will not be as heavily influenced by the polarisation current. It also means that the sign of Δ_{pol} (i.e. whether it is stabilising or destabilising) is likely to be sensitive to the physics which remains to be included in a complete model (see section 8). *If* this additional physics is unimportant, then our results indicate that the net effect of the contributions of the polarisation current from inside and outside the layer make a negligible contribution to the island evolution. In this situation, the threshold physics is likely to be dominated by the cross-field diffusion in a "transport model" [13]. We will return to this in section 8.

Additionally, the character of the plot of Δ_{pol} has changed: with ω in the $\omega_{*,e}$ direction (i.e. $\hat{\omega} > 0$) its value is no longer monotonically increasing but rises sharply for $\hat{\omega}$ close to 1 and then falls away before increasing again (see Figure 5). This suggests that the non-Maxwellian nature of the distribution function, coupled with the variation of the parameters along the flux surface, may have an important effect. For ω in the $\omega_{*,i}$ direction, the results are qualitatively similar to those obtained using the smoothing function, although the magnitude is significantly reduced.

Figure 6 shows that as $\hat{\rho}_i$ is increased, the "bump" at $\hat{\omega} \approx 1$ disappears and the character of the graph resembles that seen with the smoothing function over the full range of $\hat{\omega}$. The magnitude is, however, still significantly reduced and careful

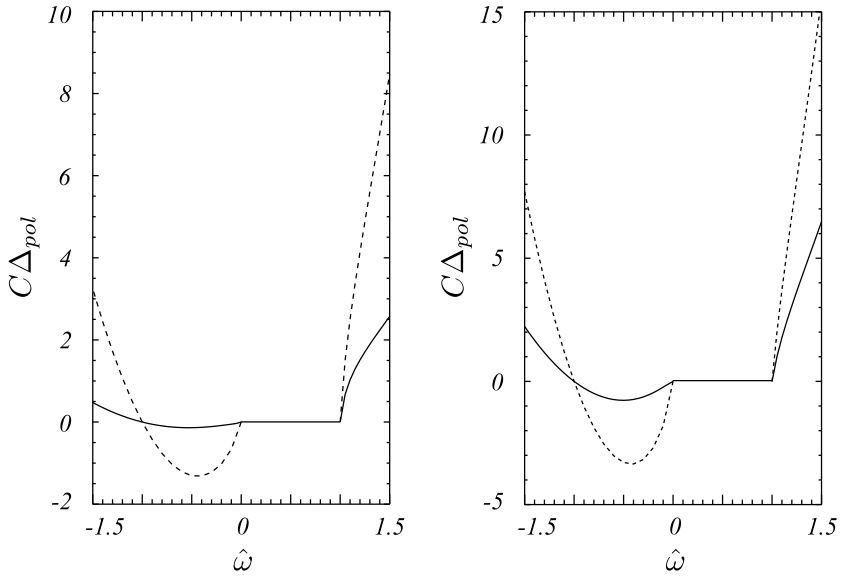

(a) The variation of Δ_{pol} with $\hat{\omega}$ for $\alpha = 10$ and $\hat{\rho}_i = 0.5$ (dashed line) compared with that obtained from including the diffusive layer.

(b) The variation of Δ_{pol} with $\hat{\omega}$ for $\alpha = 10$ and $\hat{\rho}_i = 1$ (dashed line) compared with that obtained from including the diffusive layer.

Figure 6: The effect of including the diffusive layer for two different values of $\hat{\rho}_i$. Except where stated, the values of the parameters are the same as those used in Figure 5.

examination shows that this effect is more pronounced for smaller $\hat{\rho}_i$. This suggests that for small islands (w is small and therefore $\hat{\rho}_i$ is large) the polarisation current has a reduced impact on the island growth and that as the island increases in size ($\hat{\rho}_i$ decreases), the impact decreases faster than predicted by previous models.

In summary, an important result from this work is that the contribution of the polarisation current to the island stability is significantly reduced by the inclusion of a diffusive layer at the island separatrix. A caveat is that more physics still needs to be included for a complete model before definitive conclusions can be drawn about the role of the polarisation current. In the following section we discuss some limitations in our calculation and consider the additional physics that might modify our conclusion regarding the significance of the polarisation current.

8 Discussion

In this section we discuss some potential limitations concerning our calculation. Firstly, the Fourier transform function k^2F that must be inverted has the form

$$k^2F\left(k,\theta<0,\sigma=1\right)=2\left(k-i\right)\sigma C_\sigma e^{q_l(k)}\frac{e^{k^2|\theta|}}{1+e^{\pi k^2}}, \tag{82}$$

which for $\theta=-\pi$ does not tend to zero at large k (Eq.(26) reveals that, for $\sigma=1,\theta=-\pi$ the function F tends to a constant at $k=\pm\infty$) and therefore cannot be successfully inverted: sufficiently large values of k are required to get arbitrarily close to $\theta=-\pi$. In order to deal with this, the code has been adapted so that the box width (in ξ) is variable. The bounding values of ξ then become $\pm\pi\mp\varepsilon$ instead of $\pm\pi$ and varying the small parameter ε allows the distance to the X-point to be varied and the limit $\varepsilon\rightarrow 0$ identified.

It is to be noted that, as a result of the Fourier transform's behaviour, the distribution becomes steeper and steeper until, at the X-point, the plot is discontinuous (see Figure 7(a)). Careful examination reveals that this behaviour is localised to the X-point region and that in this region $\partial f/\partial\theta$ is large, as shown in Figure 7(b). Indeed, close study of Figure 7(b) reveals that the scan does not extend all the way to the X-point at $\theta=-\pi,\Omega=1$.

The neglect of the second term in Eq.(12) made in section 3 required that

$$\frac{\partial\ln f}{\partial\psi}\gg\frac{\partial\theta}{\partial\psi}, \tag{83}$$

where it was assumed that $\partial f/\partial\theta\sim f$ and it was noted that Eq.(83) would be valid in all but a very narrow layer ($\sim e^{-w/L_r}$) surrounding the separatrix. Figure 9 shows that as ξ approaches $-\pi$ the distribution function f samples values closer and closer to the point $(\Omega=1,\theta=-\pi)$ where the spike in $\partial f/\partial\theta$ exists. The X-point itself is within this layer and the breakdown of the model in this region is not unexpected. However, the region is very narrow and so will make only a very

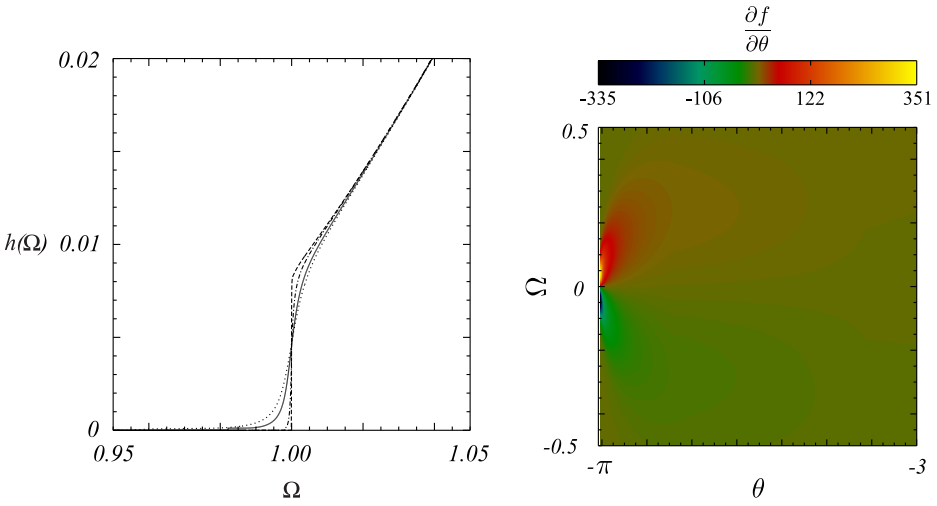

(a) The form of the density function $h(\Omega)$ as the X-point is approached. The plots are at $\xi = -3.1407$ $(--)$, $\xi = -3.1372$ $(- \cdot -)$, $\xi = -3.1345$ (full line) and $\xi = -3.1336$ $(\cdots)$.

(b) A plot of $\partial f/\partial\theta$ close to $\theta = -\pi$. Note that the minimum value of θ in this plot is $-\pi+8.84\times10^{-4}$. It can clearly be seen that as θ approaches $-\pi$ $\partial f/\partial\theta$ becomes large.

Figure 7: The breakdown in the model at the point $\theta = -\pi$; this corresponds to the island X-point.

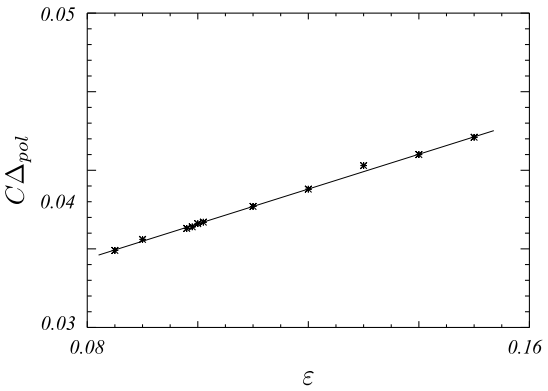

Figure 8: The numerically determined values of Δ_{pol} as the X-point is approached (i.e. the parameter ε is decreased).

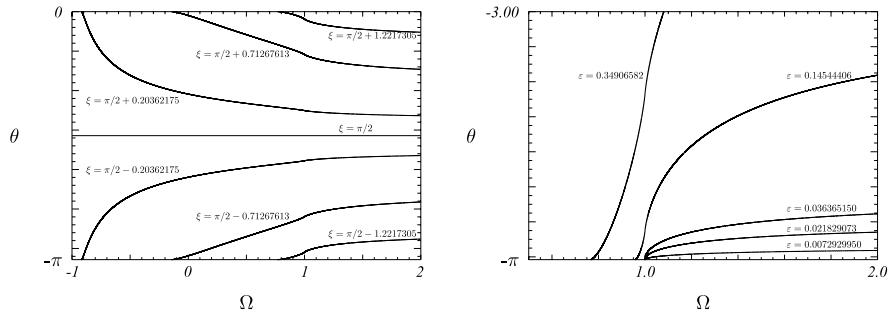

(a) The value of θ for fixed ξ and varying values of Ω.

(b) The value of θ for fixed ξ and varying values of Ω. This plot is zoomed in on the point $\theta = -\pi$, $\Omega = 1$ where the model breaks down.

Figure 9: The transformation from ξ and Ω to θ.

small contribution to Δ_{pol}, defined in Eq.(77). This assertion is supported by the convergence of Δ_{pol} as ε tends to zero (see Figure 8).

In section 3 the non-linearities associated with the parallel electric field term in the kinetic equation were not included [1] and it was remarked that this issue would be addressed a posteriori. This assumption is considered here and its likely impact on the solution assessed. Figure 10 shows a colour contour plot of $E_{\|}$ = -$\nabla_{\|}\phi$ in the separatrix region. The values are not determined at the X-points (as discussed above). However, it can be seen that the function starts to increase rapidly as the X-point is approached. It is possible that this behaviour may be due to the discontinuity in f at the X-point but the growth of $E_{\|}$ in this region is a significant issue and suggests that the electric field term may need to be fully retained in order to completely model the contribution of the polarisation current to the stability of the magnetic island. This is a topic for future research.

Finally, we remark that in a toroidally confined plasma the modifications due to trapped particle (i.e. banana) orbits could be important and modify our conclusion about the effect of the polarisation current on stability; this provides a further topic for future research.

9 Conclusions

In this paper, the effect of cross-field diffusion competing with the rapid transport along the magnetic surfaces (based on the work of reference [19] in slab geometry) , has been incorporated into an earlier kinetic model [6]; this permits a smooth matching of the density profile across the island separatrix. This earlier model, valid for arbitrary ratio of w/ρ_i, used a phenomenologically-based smoothing of

[1] Note that the adiabatic piece of the electron distribution function f arises from $v_{\|}E_{\|}\partial F_0/\partial v$, and so the $E_{\|}$ term is not completely neglected. It is actually $v_{\|}E_{\|}\partial\left(f - F_0\right)/\partial v$ that is neglected.

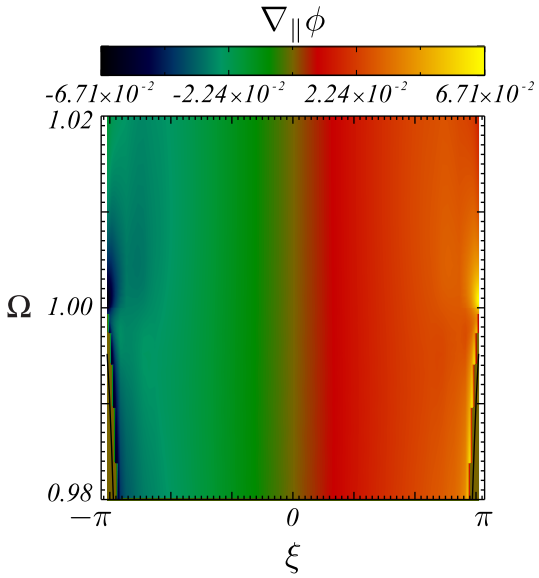

Figure 10: $\nabla_{\|}\phi$ in the separatrix region.

the density profile involving a smoothing factor α to investigate the effect of removing the discontinuity in density that appears in the absence of such diffusive effects. However the model of reference [19] predicts a non-Maxwellian electron distribution function near the island separatrix, which cannot match to the necessary Maxwellian form far from the island. To overcome this we have considered an intermediate region where collisions compete with the diffusion, thus driving the solution towards the required Maxwellian form.

As was expected, the density profile is smoothed into the island region; also it can no longer be regarded as a flux-surface quantity in the separatrix layer. The width of the transition layer over which the distribution is smoothed is related to the diffusion coefficient, D, and thus provides a basis for estimating the smoothing parameter α used earlier. This new form for the density is then used to determine the electrostatic potential and the polarisation current. From this the parameter, Δ_{pol}, characterising the effect of the polarisation current on the island stability, has been determined. The results show that the inclusion of the diffusive layer acts to reduce the magnitude of Δ_{pol}, with the difference more noticeable for islands rotating in the $\omega_{*,i}$ direction. Furthermore, the inclusion of the diffusive layer shows that the effect of the polarisation current falls off faster as the island width increases than was previously thought.

This is a particularly significant result as it suggests that the contribution to the polarisation current from the separatrix boundary layer is substantially less than previous calculations have predicted. This in turn implies that the polarisation current will not have as strong an influence on the early evolution of the magnetic island. In particular, in regions where Δ_{pol} is positive the island will not grow as

quickly. If other phenomena act to suppress the island size, this could lead to a higher threshold for island growth, a smaller saturated island or, indeed, the island disappearing altogether. Conversely, in the case where Δ_{pol} is negative, which possibly provides a threshold for growth of the island due to other mechanisms (for example, the bootstrap drive of NTMs), the threshold would be somewhat reduced if determined solely by the polarisation current. In particular, it could mean a more substantial role for the transport model [13].

However, we have already noted the potential importance of non-linearities in the parallel component of the electric field which we have not retained. It is possible that these could make a significant contribution to the island stability by modifying the polarisation current in the separatrix boundary layer. The values of $E_{\|}$ determined a posteriori suggest that the contribution will be small over most of the island but that its effect at the X-points may be significant. It is possible that this increase in magnitude could be due to the discontinuous form of the density at the island X-point resulting from the breakdown of the kinetic model at the island's X-points and the associated unphysical form of the density there. However, the convergence with the small parameter ε, representing the influence of the X-point region, and the fact that $E_{\|}$ is small, give some confidence in our predictions. Nevertheless, the fact that Δ_{pol} is significantly reduced compared to earlier theories suggests that its value and sign are sensitive to such small potential additional contributions. A comprehensive study would require a full numerical solution to the initial partial differential equation and is left to future work. Furthermore, in a toroidal plasma, the trapped ion orbits substantially modify the polarisation current. It is important to address both of these challenging theoretical issues by future research before one can draw definitive conclusions regarding the role of the polarisation current in NTM threshold physics.

Finally we emphasize that the sign of Δ_{pol} depends on $\hat{\omega}$ (see Figure 5), highlighting the importance of self-consistently determining the island rotation frequency, ω, rather than regarding it as an input parameter, as this will provide an indication of whether the polarisation current acts to stabilise or destabilise the island for a specified set of experimental parameters. Such a calculation involves torque balance considerations which depend on the $\sin\xi$ (out of phase) component of J^{pol}, and probably require non-ambipolar diffusion. Such a component could be driven by the diffusion considered here and developing the formalism to determine $\hat{\omega}$ is also a subject for future study.

Acknowledgement

We would like to thank Per Helander for his input and helpful discussions regarding this work. The work was supported by the Engineering and Physical Sciences Reseach Council and by the European Communities under the contract of Association between EURATOM and UKAEA. The views and opinions expressed herein do not necessarily reflect those of the European Commission.

References

[1] W.X. Qu and J.D. Callen. *University of Wisconsin report UWPR 85-5*, 1985.

[2] R. Carrera, R.D. Hazeltine and M. Kotschenreuther. *Phys. Fluids* **29** 899 (1986).

[3] F.L. Waelbroeck and R. Fitzpatrick. *Phys. Rev. Lett.* **78** 1703 (1997).

[4] F.L. Waelbroeck, J.W. Connor and H.R. Wilson. *Phys. Rev. Lett.* **87** 215003 (2001).

[5] R. Fitzpatrick, F. L. Waelbroeck and F. Militello. *Phys. Plasmas* **13** 122507 (2006).

[6] M. James and H.R. Wilson. *Plasma Phys. Controlled Fusion* **48** 1647 (2006).

[7] H.R. Wilson, J.W. Connor, R.J. Hastie, and C.C. Hegna. *Phys. Plasmas* **3** 248 (1996).

[8] A.I. Smolyakov, A. Hirose, E. Lazzaro, G.B. Re and J.D. Callen. *Phys. Plasmas* **2** 1581 (1995).

[9] R. Fitzpatrick, P.G. Watson and F. L. Waelbroeck. *Phys. Plasmas* **12** 082510 (2005).

[10] P.H. Rebut and M. Hugon. *Plasma Phys. Controlled Fusion* **33** 1085 (1991).

[11] E. Poli, A Bergmann and A. G. Peeters. *Phys. Rev. Lett.* **94** 205001 (2005).

[12] Z. Chang, J.D. Callen, E.D. Fredrickson, R.V. Bundy, C.C. Hegna, K.M. McGuire, M.C. Zarnstorff, and TFTR group. *Phys. Rev. Lett.* **74** 4663 (1995).

[13] R. Fitzpatrick. *Phys. Plasmas* **2** 825 (1995).

[14] N.N Gorelenkov, R.V. Budny, Z. Chang, M.V. Gorelenkova and L.E. Zakharov. *Phys. Plasmas* **3** 3379 (1996).

[15] D.J. Grove and D.M. Meade. *Nucl. Fusion* **25** 1167 (1985).

[16] O. Sauter, R J Buttery, R Felton, T C Hender, D F Howell et al. *Plasma Phys. Controlled Fusion* **44** 1999 (2002).

[17] S Guenter et al. *Nucl. Fusion* **38** 1431 (1998).

[18] R.J. Lahaye. *Phys. Plasmas* **13** 055501 (2006).

[19] R.D. Hazeltine, P. Helander and P.J. Catto. *Phys. Plasmas* **2** 2920 (1997).

[20] P.H. Rutherford. *Phys. Fluids* **16** 1903 (1973).

Appendix: Calculation of the polarisation current

Quasi-neutrality is used to equate the ion and electron responses which, after some manipulation [6], yields,

$$\hat{\phi} \;=\; \frac{\hat{\omega}\tau+1}{\hat{\omega}-1}\bar{\phi} - \frac{w}{L_n}\left(\hat{\omega}-1\right)\left(X-h\left(\Omega,\xi\right)\right) \tag{A1}$$

The ion response is given by Eq.(A2):

$$\delta n_i \;=\; -n_0\tau\hat{\phi} + n_0\frac{\hat{\omega}\tau+1}{\hat{\omega}}\hat{\phi}_i \tag{A2}$$

Calculating the plasma current by integrating the ion and electron gyro-kinetic equations over velocity space yields:

$$k_\parallel \left.\frac{\partial J_\parallel}{\partial \xi}\right|_\Omega = n_0 e\omega_{*,e}\left.\frac{\partial\hat{\phi}}{\partial\xi}\right|_x - e\hat{\omega}\omega_{*,e}\left.\frac{\partial}{\partial\xi}\right|_x\left(\delta n_i\right)$$

$$+\frac{cT_e}{B_0}\left(\boldsymbol{\nabla} z\times\boldsymbol{\nabla}\hat{\phi}\right)\cdot\boldsymbol{\nabla}\left(\delta n_i\right) \tag{A3}$$

Here we have defined $X = x/w$, $\hat{\omega} = \omega/\omega_{*,e}$, $\tau = T_e/T_i$, $e = q_i = -q_e$, $\hat{\phi} = (e/T_e)\phi$, $\hat{\phi}_i = (e/T_e)\phi_i$ and $\bar{\phi} = \hat{\phi}_i - \hat{\phi}$. Using Eq.(A2) the density can be eliminated from Eq.(A3) and, substituting $\hat{\phi}$ from Eq.(A1), results in

$$\frac{1}{n_0 e c_s}\boldsymbol{\nabla}_\parallel J_\parallel = -4\frac{L_s}{L_n}\frac{\rho_s}{w}\left(\hat{\omega}\tau+1\right)\frac{\partial h}{\partial\Omega}\boldsymbol{\nabla}_\parallel\bar{\phi} + 4\frac{L_s}{L_n}\frac{\rho_s}{w}\left(\hat{\omega}\tau+1\right)\frac{\partial\bar{\phi}}{\partial\Omega}\boldsymbol{\nabla}_\parallel h\left(\Omega,\xi\right), \tag{A4}$$

This equation can be integrated to give

$$\frac{1}{n_0 e c_s}J_\parallel = 4\frac{L_s}{L_n}\frac{\rho_s}{w}\left(\hat{\omega}\tau+1\right)\int d\xi\left[\frac{\partial\bar{\phi}}{\partial\Omega}\frac{\partial h}{\partial\xi} - \frac{\partial h}{\partial\Omega}\frac{\partial\bar{\phi}}{\partial\xi}\right] + K(\Omega). \tag{A5}$$

where the integral is performed at constant Ω. The constraint from Ohm's law, namely that $\left\langle J_\parallel^{pol}\right\rangle_\Omega = 0$, is employed to determine the arbitrary flux function, $K(\Omega)$, arising in this integration. The final form of the current is then

$$\frac{1}{n_0 e c_s}J_\parallel = 4\frac{L_s}{L_n}\frac{\rho_s}{w}\left(\hat{\omega}\tau+1\right)\left[I_J - \langle I_J\rangle_\Omega\right] \tag{A6}$$

where

$$I_J = \int_0^\xi d\xi'\left[\frac{\partial\bar{\phi}}{\partial\Omega}\frac{\partial h}{\partial\xi'} - \frac{\partial h}{\partial\Omega}\frac{\partial\bar{\phi}}{\partial\xi'}\right]. \tag{A7}$$

Since h is no longer a flux surface function, the evaluation of the above integral cannot be performed analytically and must instead be performed numerically.